IEEE Access
Multidisciplinary | Rapid Review | Open Access Journal

Received July 14, 2020, accepted August 8, 2020, date of publication August 17, 2020, date of current version August 27, 2020.

Digital Object Identifier 10.1109/ACCESS.2020.3017102

Analysis of a Brushless Wound Rotor Synchronous Machine Employing a Stator Harmonic Winding

GHULAM JAWAD SIREWAL[1], MUHAMMAD AYUB[1,2], SHAHID ATIQ[3], (Member, IEEE), AND BYUNG-IL KWON[1], (Senior Member, IEEE)

[1]Department of Electrical and Electronic Engineering, Hanyang University, Ansan 426-791, South Korea
[2]Department of Electronic Engineering, Balochistan University of Information Technology, Engineering and Management Sciences, Quetta 87300, Pakistan
[3]Department of Electrical Engineering, Khwaja Fareed University of Engineering and Information Technology, Rahim Yar Khan 64200, Pakistan

Corresponding author: Byung-Il Kwon (bikwon@hanyang.ac.kr)

This work was supported in part by the BK21PLUS Program through the National Research Foundation of Korea within the Ministry of Education, and in part by the National Research Foundation of Korea (NRF) grant funded by the Korea government (Ministry of Science) (NRF-2020R1A2B5B01002400).

ABSTRACT This study proposes a new topology for brushless operation of a wound rotor synchronous machine (WRSM) employing a stator harmonic winding. It is based on generating an additional six-pole magneto-motive force component without the use of an inverter. In this topology, six thyristor switches are used to create harmonic currents for brushless operation of the machine. The usage of stator harmonic winding has the advantage of configuring the winding for six poles or any other combination based on the output requirement. In the proposed topology, a six-pole winding arrangement is used to generate a six-pole air-gap flux component aimed at rotor excitation for brushless operation. On the rotor side, two windings, namely rotor harmonic winding (to intercept the air-gap harmonic flux) and field winding, along with a diode rectifier are mounted. 2-D finite element analyses and experiments were carried out to analyze the brushless operation of the WRSM.

INDEX TERMS Brushless operation, harmonic excitation, synchronous machine, wound rotor.

I. INTRODUCTION

The problems of demagnetization and increased cost associated with rare earth magnets in permanent magnet synchronous machines have encouraged researchers to use wound rotor synchronous machines (WRSMs) as they are particularly suitable for automotive applications [1]. However, in applications where low-capacity WRSMs are used owing to their low-cost advantage, an inherent problem is faced regarding the assembly of brushes and slip rings. Nevertheless, WRSMs can still be used in low-capacity machines by operating them without an assembly of brushes and slip rings [2]–[5].

The problem has been addressed in many research articles. A design approach aimed at the recovery of space harmonic power was investigated in recent years as an efficient method using, for example, field poles excited by space harmonics [6].

The associate editor coordinating the review of this manuscript and approving it for publication was Gaolin Wang.

Similarly, a self-excited brushless synchronous generator, which employed a fifth harmonic of armature magneto-motive force (MMF) to excite the main field winding has been introduced and analyzed in [7]. This topology is heavily dependent on space harmonics and residual magnetism which can lead to voltage build-up and regulation difficulties.

Additionally, current injection by an additional inverter to create harmonics from stator windings has also been used in recent research. Distributed windings have been used in these topologies to avoid problems related to residual magnetism [8]–[10].

In [8], brushless excitation was achieved by employing an additional third harmonic current injection from another inverter in the same stator winding. This resulted in a temporarily pulsating third harmonic MMF in conjunction with the fundamental rotating MMF in the air-gap. The harmonic component was used to excite the rotor winding by inducing a voltage in the rotor-mounted harmonic winding. The induced voltage was rectified using a diode rectifier, which was also

mounted on the rotor, and a DC voltage was fed to the field winding.

In [9], the same third harmonic current excitation topology was used with a dual inverter topology where dual three-phase armature windings were used and a third harmonic component of current was injected through a neutral point connected between both armature windings. However, these topologies are expensive as the drive requires an additional inverter for injecting the third harmonic current to the stator windings as in [8].

Alternatively, two three-phase currents were supplied to the two different parts of the stator windings by two inverters in another brushless WRSM topology. Both inverters were controlled to supply different current magnitudes to the two different parts of the stator winding to generate a fundamental and a subharmonic component of stator MMF for torque and rotor excitation [11]. However, an additional inverter is required to supply a different current magnitude to generate subharmonic MMF, which means the topology is valid for only two-inverter topologies. Although, single inverter topologies have been proposed that are based on the excitation principle of [11], these topologies lack the wider flux-weakening capabilities undermining the advantage of field control ability of the WRSM [3], [12]–[14].

In 2016, six-thyristor switch controlled scheme was proposed for brushless excitation as shown in Fig. 1(a). In which scheme the thyristor switches are turned on before zero crossing of the current and the switches are turned off at zero current crossing. Consequently, avoiding used of the commutation circuit components or any additional input source for generating third harmonic currents [15]. However, the machine has high torque ripple factor emerging from unwanted harmonics due to non-sinusoidal winding currents.

For the same purpose of generating an excitation MMF, a harmonic component generation scheme was developed for brushless excitation system as shown in Fig. 1 (b). The stator MMF for excitation purpose is created by controlled input current to an additional stator winding through a two-leg inverter. In this case the excitation current is received from a transformer at the output terminals of the same machine. Since the harmonic current is in the additional winding, it is inherently decoupled in the air gap field reducing unwanted harmonic effects [10]. However, controlled harmonic current fed to the additional stator winding makes the system complicated.

Both the schemes work well with their respective limitations. However, advancement has been made in this regard to address the prevalent brushless excitation problems by dual inverter schemes using conventional dual inverters with open phase armature windings [9], where zero-sequence phase-shifted current can be injected to induce voltage in the rotor's harmonic winding at different speeds for motoring purpose.

In 2019, a combined design with main machine and embedded synchronous exciter was developed as a robust structure which utilizes conventional drive components for

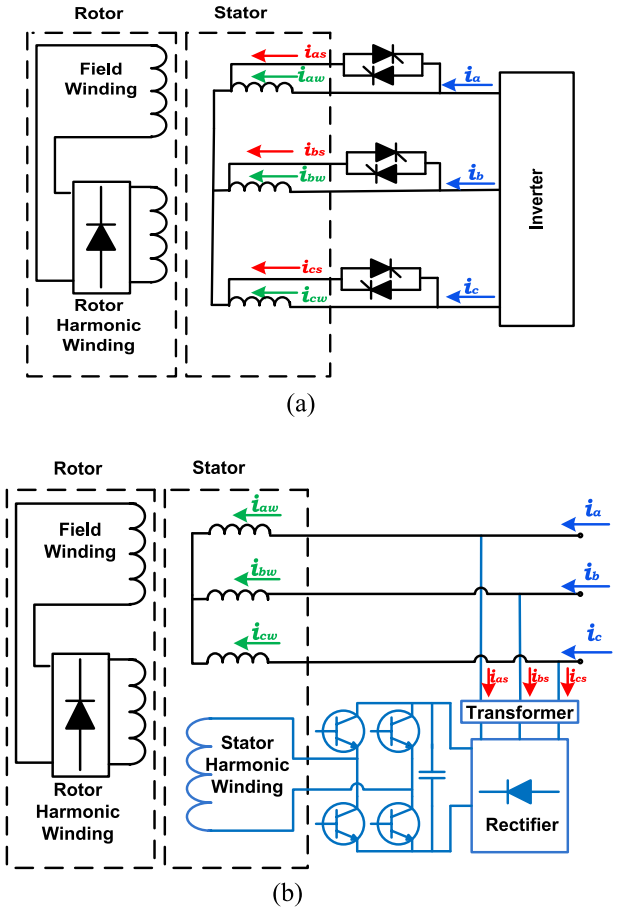

FIGURE 1. Schematic diagram of existing topologies (a) basic topology for brushless WRSM using thyristor switches [15] and (b) brushless synchronous machine with stator harmonic winding [10].

flux control. The system is advantageous in that it uses conventional drive system components. However, the machine structure is volumetric and only small machines can be designed with this proposed system [5], [20].

In 2020, dual-inverter-controlled scheme was proposed based on open armature winding pattern with time-controlled current transmission using inverter reference current modification to generate third harmonic current component [18], [19].

Referring to Fig. 1 (a) the brushless WRSM (BL–WRSM) topology has the disadvantage of using the third harmonic current in the same armature winding to induce a voltage in the rotor harmonic winding resulting in high harmonics which eventually needs a machine structure optimization. The harmonics eventually contribute to high torque ripple of the machine. Additionally, the inverter and switches are combined to produce two main components of the air gap field.

This paper proposes a BL–WRSM topology that employs a stator harmonic winding. Compared to the existing topology illustrated in Fig. 1 (b) [10], the proposed topology consists of thyristor switches which turn off naturally at zero-crossing

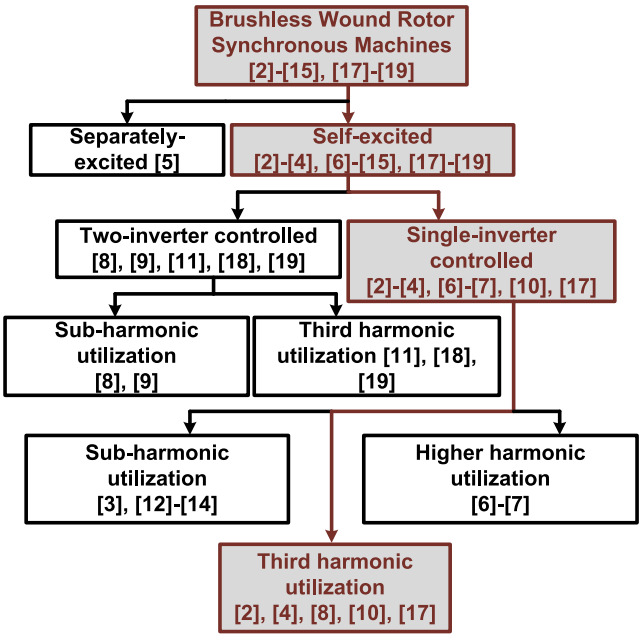

FIGURE 2. Classification tree of brushless wound rotor synchronous machines based on excitation.

of current. Additionally, since the neutral wire is connected to the rectifier and forms a closed loop, transformer is not needed unlike the existing topology. Therefore, the overall brushless WRSM size is reduced saving cost and reducing components' power loss.

Compared to the existing topology illustrated in Fig. 1 (a) [15], the proposed topology has reduced harmonics content, lower power loss in electromagnetic conversion. Whereas, compared to the topology shown in Fig. 1 (b) [10], transformer is removed and transistors are not used which require commutation circuit.

A 2-D finite-element analysis (FEA) is performed to analyze and verify the operating principle of the proposed BL–WRSM. To support the theory and working of the topology, and experiment on rated load on a prototype machine is also performed. An overall categorization of brushless WRSMs based on excitation is given in a tree-form of classification for simple understanding in Fig. 2.

II. PROPOSED TOPOLOGY AND WORKING PRINCIPLE

A. PROPOSED TOPOLOGY

The schematic of the proposed topology is based on the stator harmonic winding utilization. The proposed topology diagram is shown in Fig. 3.

There are two windings on the stator, the general three-phase winding with a four-pole arrangement, and a stator harmonic winding with a six-pole arrangement. To decouple the air gap flux interaction, the six-pole stator harmonic winding generates a pulsating six-pole flux which does not interact with the rotating four pole flux. Two antiparallel thyristor switches are connected in parallel with each phase winding. The thyristor switches are closed near the zero crossing, and

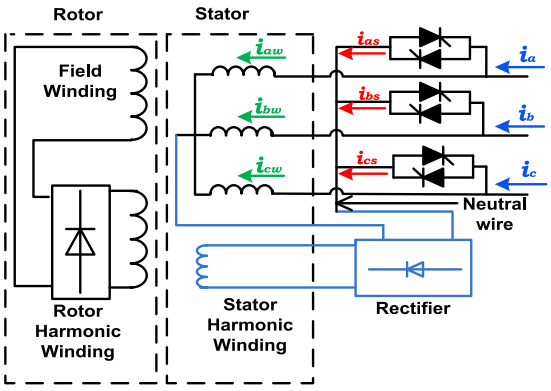

FIGURE 3. Schematic diagram of the proposed topology.

a zero-sequence current is generated in the switches. This zero-sequence current is rectified by the stator's rectifier, and a DC current is fed to the stator harmonic winding of the six-pole configuration.

There are two windings on the rotor, a four-pole field winding, and a six-pole rotor harmonic winding. Both the harmonic and the field windings were connected by a diode bridge rectifier which was also mounted on the rotor. The six-pole flux generated in the air-gap owing to the current in the stator harmonic winding induces a voltage in the rotor harmonic winding. The current flowing in the rotor harmonic winding owing to the induced voltage is rectified and fed to the field winding. Consequently, brushes and slip rings are not needed, and brushless operation is achieved. A 2–D layout of the machine for the proposed topology is shown in Fig. 4. The stator winding is a double layer used to fix the three-phase armature windings, and the additional stator harmonic winding is indicated with the symbol "Hs." The stator harmonic winding is fitted in 12 slots with a distributed six-pole arrangement. On the rotor side, two types of windings are mounted, namely field winding with a four-pole concentrated arrangement, and a rotor harmonic winding with a six-pole concentrated arrangement. Table 1 shows the parameters of the machine structure depicted in Fig. 4. The stator and rotor structure of the machine are shown in Fig. 4 (a) and (b) respectively. In the stator there are three-phase coils and a stator harmonic winding. The patterns of the three-phase coils configured for four poles and the stator harmonic winding configured for six poles are illustrated in Fig. 4 (c). In the rotor there are two windings, namely the rotor harmonic winding and the field winding. Fig. 4 (d) illustrates the patterns of the rotor harmonic winding configured for six poles and the field winding configured for four poles.

B. WORKING PRINCIPLE FOR BRUSHLESS OPERATION

The proposed brushless topology works based on the basic principle of the WRSM. In addition, the topology generates harmonic currents that are used for rotor excitation for brushless operation. To create a rotating MMF, a WRSM is fed with the three-phase line currents from the inverter.

TABLE 1. Machine design parameters.

Unit	Parameters	Value
kW	Rated power	1
Nm	Rated torque	4.6
rpm	Rated speed	1800
A-peak	Rated current	7
mm	Stator's outer diameter	177
mm	Rotor's outer diameter	99
mm	Air-gap length	0.5
mm	Shaft diameter	24
mm	Stack length	65
-	Number of poles	4
-	Number of stator slots	18
-	No. of stator harmonic winding poles	6
-	Armature winding turns	336
-	Stator harmonic winding turns	168
-	Field winding turns/pole	110
-	Rotor harmonic winding turns/pole	64/6

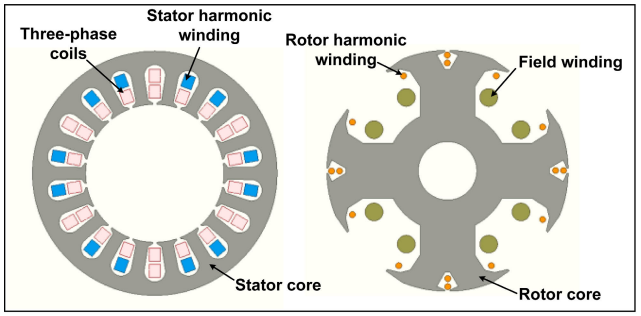

FIGURE 4. Machine structure: (a) 18-slot stator and windings, (b) Rotor with four-pole field winding and six-pole rotor harmonic winding, (c) stator windings arrangement, and (d) Rotor windings arrangement.

The three-phase line currents in the conventional WRSM are

$$\left.\begin{aligned} i_a &= I\cos\omega t \\ i_b &= I\cos\left(\omega t - \frac{2\pi}{3}\right) \\ i_c &= I\cos\left(\omega t + \frac{2\pi}{3}\right) \end{aligned}\right\} \quad (1)$$

where I, is the peak value of line current, ω is the angular electrical frequency, and t is time. In the brushless WRSM, each line current is divided into coil current and switch current. Therefore, the coil current responsible for generating the rotating MMF is given by

$$\left.\begin{aligned} i_{aw} &= i_a - i_{as} \\ i_{bw} &= i_b - i_{bs} \\ i_{cw} &= i_c - i_{cs} \end{aligned}\right\} \quad (2)$$

where i_{aw}, i_{bw}, and i_{cw}, represent the coil currents and i_{as}, i_{bs}, and i_{cs}, represent the switch currents. The currents which flow through the switches of the three phases are such that the current in each switch has a value during the switching period only. When the thyristor pulse is positive and equal to 1 V, an instantaneous current flows through the switch. In all other cases, this current is zero. For simplicity, a general pulse train equation is considered to know the thyristor has been turned on. Theoretically, the function that defines the "on" state of the thyristor switch which is in parallel with the winding of phase A is given by

$$f_a(t) = \frac{\tau}{T} + \sum_{n=1}^{\infty} \frac{2}{n\pi} \sin\left(\frac{\pi n\tau}{T}\right) \cos\left(\frac{2\pi n}{T}\left(wt - \frac{\tau}{2}\right)\right) \quad (3)$$

where τ is the duration of the on state of the thyristor, T is the time period. To ensure that the pulse frequency is twice that of the current frequency, t is replaced with $2t$. As the "on" states for the switches connected with phases B and C occur at the angles of $-2\pi/3$ and $+2\pi/3$ respectively, the "on" state functions for the switches are then calculated as

$$\begin{aligned} f_a(t) &= \frac{\tau}{T} + \sum_{n=1}^{\infty} \frac{2}{n\pi} \sin\left(\frac{\pi n\tau}{T}\right) \cos\left(\frac{2\pi n}{T}\left(\omega t - \frac{\tau}{2}\right)\right) \\ f_b(t) &= \frac{\tau}{T} + \sum_{n=1}^{\infty} \frac{2}{n\pi} \sin\left(\frac{\pi n\tau}{T}\right) \cos\left(\frac{2\pi n}{T}\left(\omega t - \frac{\tau}{2} - \frac{2\pi}{3}\right)\right) \\ f_c(t) &= \frac{\tau}{T} + \sum_{n=1}^{\infty} \frac{2}{n\pi} \sin\left(\frac{\pi n\tau}{T}\right) \cos\left(\frac{2\pi n}{T}\left(\omega t - \frac{\tau}{2} + \frac{2\pi}{3}\right)\right) \end{aligned} \quad (4)$$

Herein, the independent variable for the phase current and on state function is t, and T is half the time period of the sine current.

The coil current, switch current, and line current for phase A are illustrated in Fig. 5. When the thyristor is triggered, the coil current drops to zero and at the same time the switch current rises to a value of line current at that instant.

As pure sine wave currents are fed to the machine windings, the harmonic current flows in the closed loop between the switch connected to the stator harmonic winding and the coils of phase A when the thyristor is turned on. Neglecting the transient current, the switch currents for the three phases are calculated as

$$i_{as} = \begin{cases} 0 & \text{if } f_a(t) = 0 \\ I\cos(\omega t) & \text{if } f_a(t) \neq 0 \end{cases}$$

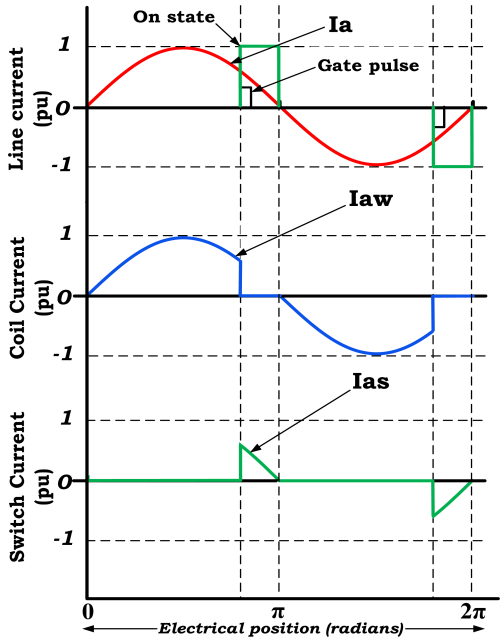

FIGURE 5. Illustration of current waveforms resulting from switching on thyristors before zero crossing.

$$i_{bs} = \begin{cases} 0 & \text{if } f_b(t) = 0 \\ I\cos(\omega t - 2\pi/3) & \text{if } f_b(t) \neq 0 \end{cases}$$
$$i_{cs} = \begin{cases} 0 & \text{if } f_c(t) = 0 \\ I\cos(\omega t + 2\pi/3) & \text{if } f_c(t) \neq 0 \end{cases} \quad (5)$$

These currents add up and flow in the neutral wire. This means that the neutral current is

$$i_n = i_{as} + i_{bs} + i_{cs} \quad (6)$$

By substituting (5) for switch currents in (2) we obtain:

$$i_{aw} = \begin{cases} I\cos(\omega t) & \text{if } f_a(t) = 0 \\ 0 & \text{if } f_b(t) \neq 0 \end{cases}$$
$$i_{bw} = \begin{cases} I\cos(\omega t - 3\pi/3) & \text{if } f_b(t) = 0 \\ 0 & \text{if } f_b(t) \neq 0 \end{cases}$$
$$i_{cw} = \begin{cases} I\cos(\omega t + 3\pi/3) & \text{if } f_c(t) = 0 \\ 0 & \text{if } f_c(t) \neq 0 \end{cases} \quad (7)$$

The coil currents, which are responsible for creating a four-pole rotating flux to interact with the field winding flux for torque production, are calculated using (7). Equations (5) and (6) are used to calculate the switch currents to be rectified and fed to stator harmonic winding for six-pole air-gap flux production. Hence, the six-pole flux will be used to induce current in the rotor harmonic winding to be fed to the field winding for brushless operation.

Therefore, for the purpose of this analysis, the approximations of coil currents and rectified stator harmonic winding current are used to calculate the MMF for four-pole and six-pole components respectively.

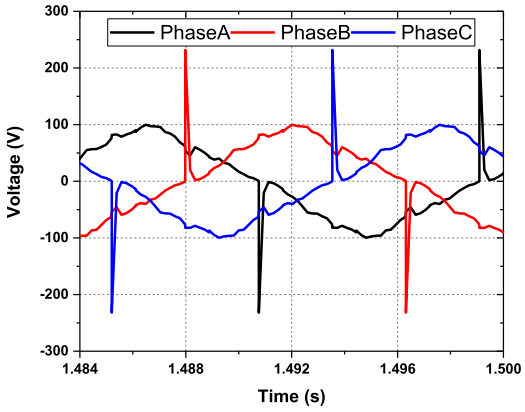

FIGURE 6. Voltage variations of the three phases.

An approximation of the coil currents can be achieved by neglecting the harmonic current using (8).

$$\left.\begin{aligned} i_{aw} &= \sqrt{2}I'_{rms}\cos\omega t \\ i_{bw} &= \sqrt{2}I'_{rms}\cos\left(\omega t - \frac{2\pi}{3}\right) \\ i_{cw} &= \sqrt{2}I'_{rms}\cos\left(\omega t + \frac{2\pi}{3}\right) \end{aligned}\right\} \quad (8)$$

where I'_{rms} is the rms value of the coil current. From these currents the fundamental MMF can be calculated as

$$F_{abc} = \frac{3N\sqrt{2}}{\pi p} I'_{rms}\cos\left(\omega t - \frac{p}{2}\theta_s\right) \quad (9)$$

where N is the phase winding turns, p is the pole pair number, and θs is the spatial position angle.

The approximation of the rectified average current fed to the stator harmonic winding neglecting the harmonic current, can be given by [16]

$$I_{Hs} = \frac{3\sqrt{3}\mathrm{V}_m}{\pi Z_{Hs}}\cos(\alpha) \quad \text{when } \alpha \leq \frac{\pi}{3} \quad (10)$$

where $\mathrm{I_{Hs}}$ is the current in the stator harmonic winding, $\mathrm{V_m}$ is the maximum rectified voltage, $\mathrm{Z_{Hs}}$ is the impedance of the stator harmonic winding and α is the firing angle. Therefore, the highest magnitude component of the MMF due to this current can be calculated by [17]

$$F_{Hs} = \frac{2N_{Hs}}{\pi p_H} I_{Hs} k_w \cos\left(\frac{p_H}{2}\theta_s\right) \quad (11)$$

where $\mathrm{N_{Hs}}$ is the number of turns of the stator harmonic winding and $\mathrm{P_H}$ is the pole pair number of the stator harmonic winding and $\mathrm{k_w}$ is the winding factor. For the brushless operation of the machine it is necessary that the air-gap MMF must have fundamental and harmonic components. Therefore, (9) and (11) show that two components are present in the air-gap flux. The fundamental four-pole MMF to synchronize with field winding flux is calculated using (9). The harmonic six-pole MMF to induce a voltage in the rotor harmonic winding is calculated using (11). As the voltage is induced in the rotor harmonic winding, it feeds current to the field winding. Hence brushless operation can be achieved.

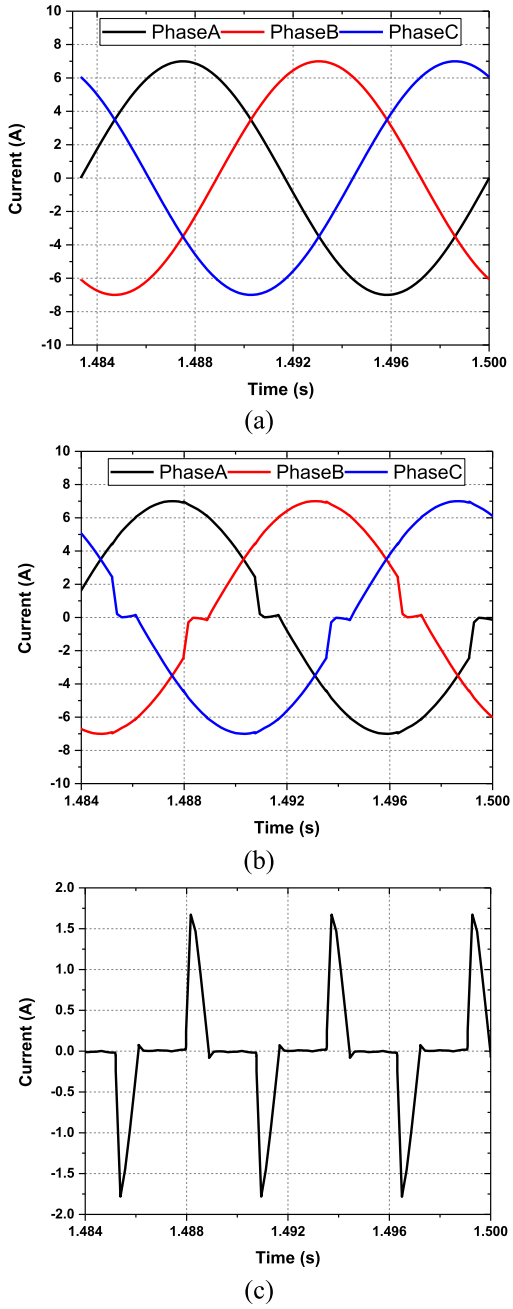

FIGURE 7. (a) Three-phase line currents. (b) Three-phase coil currents. (c) Neutral current flowing through the thyristor switches.

III. ELECTROMAGNETIC PERFORMANCE

The proposed topology was analyzed using the FEA tool ANSYS Maxwell 19.0. The phase voltages are shown in Fig. 6, and the voltages had RMS values equal to 67 V in each phase. It can be seen that voltage spikes occur at the instant of switching in Fig. 6. The voltage increases rapidly at these instances only limited by impedance of the coil because the current through coil approaches to zero at the time of switching. To limit these spikes, a voltage limiting circuit can be used across the switch, particularly when the ''on'' state is amplified for higher excitation current. In this regard, a

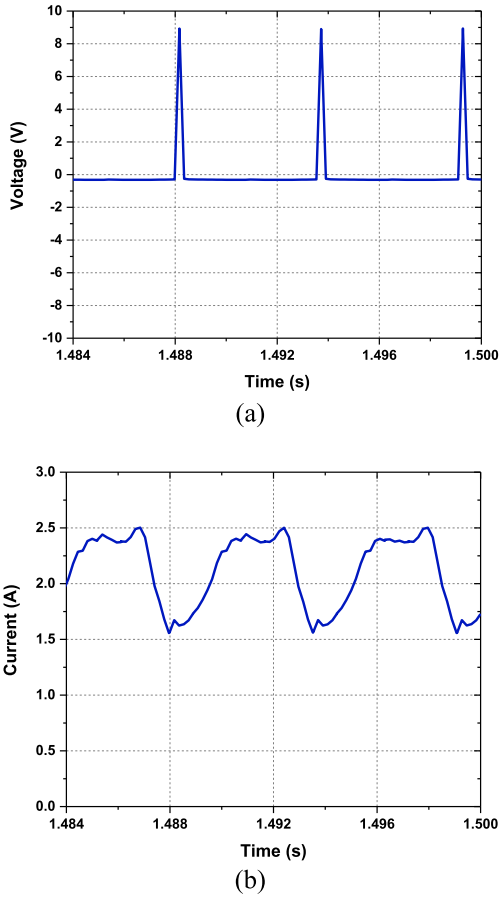

FIGURE 8. Plots of temporarily varying (a) voltage and (b) current of the stator harmonic winding.

capacitor in series with a resistor can be used as cost-effective and simple configuration of voltage limiting circuit.

The machine was fed with the three-phase line currents sinusoidal shape as shown in Fig. 7 (a), divided into coil current and neutral current as shown in Fig. 7 (b) and (c) respectively. The line current, coil current, and neutral current shown in Fig. 7 were consistent with (1), (5), and (6) respectively. Apart from the fact that the transient current is neglected in the equations, the results matched the prediction of the equations. It should also be noted that the winding impedance will affect the results if a low resistance is considered. This is due to the inductive effect of the winding which may change the magnitude of the stator harmonic winding current and the resulting air gap harmonic flux.

As the neutral current was alternating, this current would not produce the six-pole flux directly. Therefore, the currents flowing into the thyristor switches from the three-phase armature windings were rectified before they were fed into the stator harmonic winding. Depending on the ''on'' state duration of the switch, the magnitude of the harmonic current could be increased or decreased. In this analysis, the average value of the rectified current was calculated to be 2.4 A which is 16% of the three phase input current. The rectified voltage is 1.65 V which is 2.62% of the phase voltage. The waveform

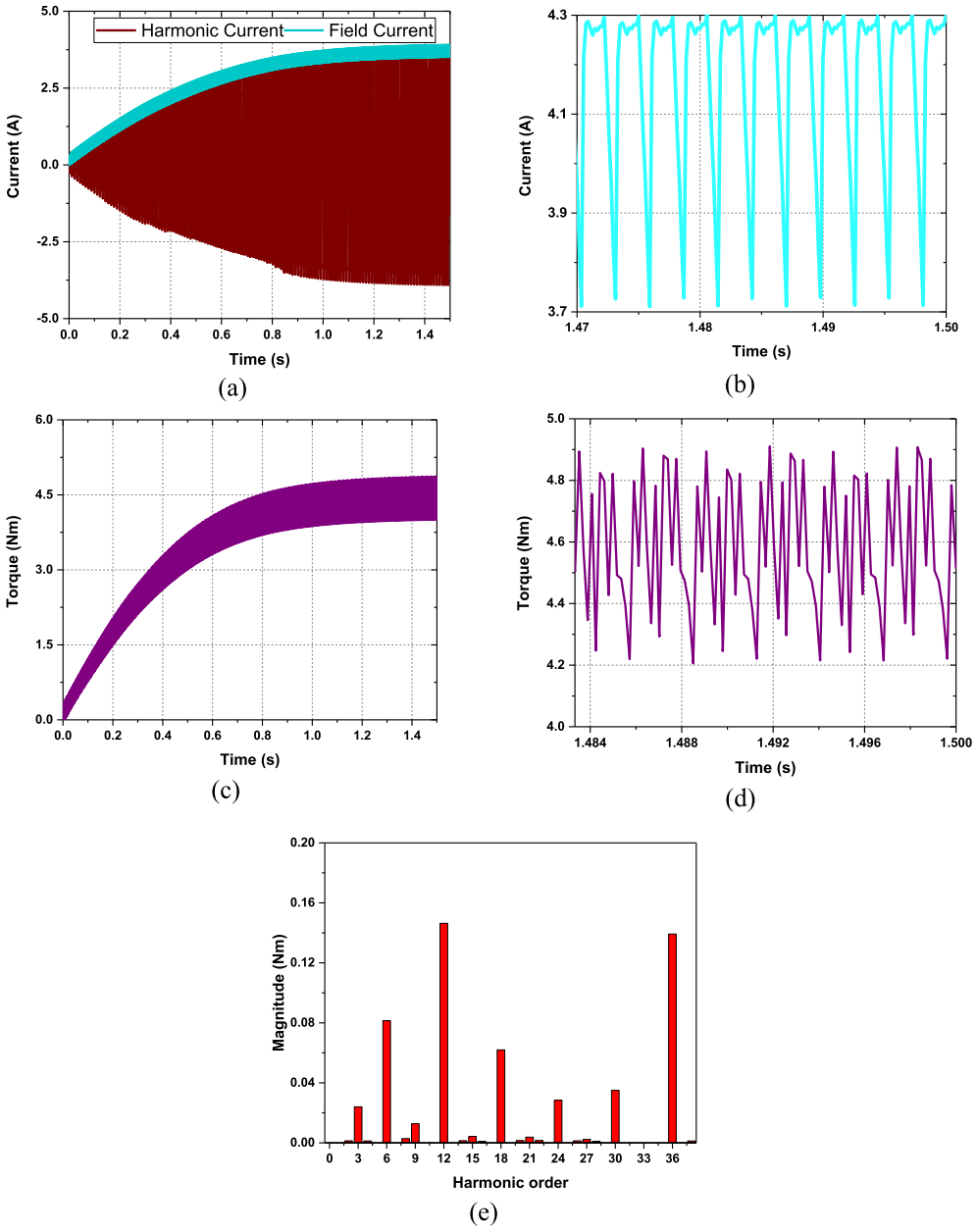

FIGURE 9. Load analysis: (a) Rotor currents (b) Field current in steady-state condition (c) Output torque (d) Torque graph in steady-state condition (e) FFT of the steady-state torque.

of the rectified voltage and current of the stator harmonic winding are shown in Fig. 8 (a) and (b), respectively.

The current in the stator harmonic winding created a six-pole flux in the air-gap which was intercepted by the rotor harmonic winding. Consequently, an AC voltage was induced in the rotor harmonic winding. Owing to this voltage, the currents in the rotor harmonic winding and the field winding gradually increased from zero to a steady state condition as shown in Fig. 9 (a). The steady-state field current graph is also shown in Fig. 9 (b) where average value of 4 A is achieved. As the field current gradually built up, the torque also proportionally increased, as shown in Fig. 9 (c). The torque in the simulation was 4.6 Nm with a torque ripple percentage of 15% as illustrated in Fig. 9 (d). The average torque and torque ripple percentage are calculated by

$$\left.\begin{aligned} T_{avg} &= \frac{T_{max} + T_{min}}{2} \\ T_{rip} &= \frac{T_{max} - T_{min}}{T_{avg}} \times 100 \end{aligned}\right\} \tag{12}$$

where Tavg is the average torque, Tmax is the maximum torque, Tmin is the minimum torque, and Trip is the torque ripple percentage. Additionally, the torque ripple harmonic frequencies are shown in Fast-Fourier-Transform (FFT) graph of Fig. 9 (e). It can be seen that the ripple is mostly generated due to 6th and multiple of 6th order

harmonics. One of the factors contributing to the 6th order torque ripple is tooth harmonic fields which depends on the structure of the machine. When the rotor field winding is intercepted by tooth harmonic fields, a voltage is induced in the field winding which allows a current flow through diode rectifier. However, it can be reduced by optimizing the structure of the machine.

As it is mentioned that the proposed topology reduces the harmonics compared to the basic topology in Fig. 1 (a) [15], the harmonic contents of both the topologies are compared in Fig. 10. Fig. 10 (a) shows the harmonic current frequency in the phase A coil and Fig. 10 (b) shows the harmonic voltage frequency in the rotor harmonic winding. It can be seen that the harmonic contents of the phase A coil current in the basic and proposed topologies is very small. However, when the voltage was induced in the rotor harmonic winding, it contained higher harmonic contents for the basic topology as opposed to the proposed topology. It can also be noted that the machine structure is such that the field pole teeth are split to accommodate rotor harmonic winding.

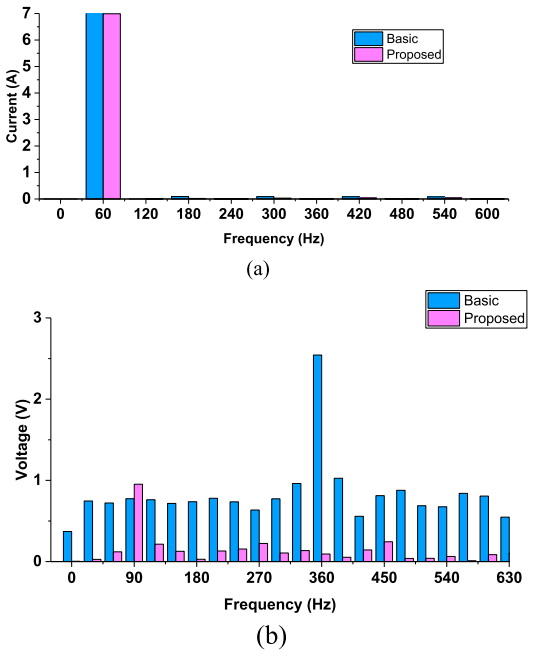

FIGURE 10. Basic and proposed topology harmonic contents: (a) Harmonic current frequency in phase A coil and (b) Harmonic voltage induced in rotor harmonic winding.

This causes a light difference in flux distribution at the pole teeth on the air gap side. For analysis the flux density and flux lines distribution at steady-state condition are shown in Fig. 11 (a) and (b) respectively.

Cogging torque of the machine is also shown in Fig. 12, when DC 4A current was fed to the machine at no-load condition.

IV. EXPERIMENT

The experiment was conducted to confirm the simulation results obtained in the FEA and hence validate the brushless

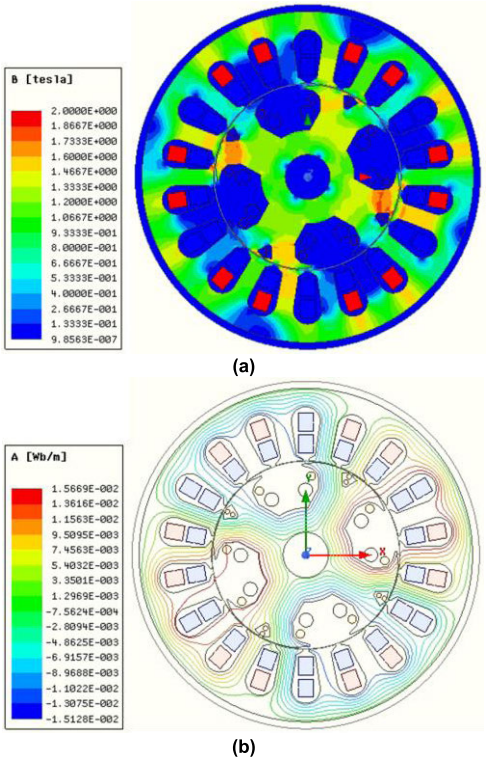

FIGURE 11. Steady-state condition plots: (a) flux density distribution and (b) flux lines distribution.

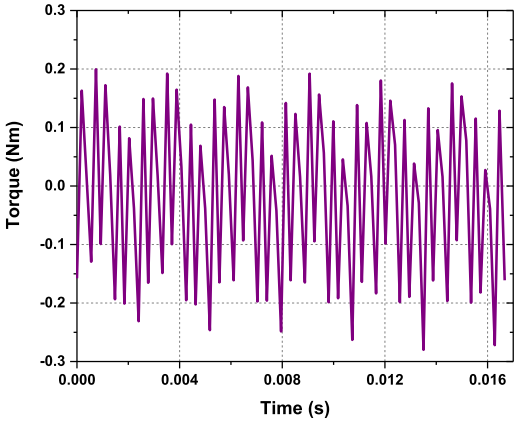

FIGURE 12. Cogging torque of the machine at 4A field current.

operation of the proposed topology. For this purpose, a prototype machine was manufactured which is shown in Fig. 13. Fig. 13 (a) and (b) show the stator and rotor core with windings respectively. In the experiment, the armature coils were supplied with controlled current from an inverter. For the brushless operation, thyristor switching was performed to feed the harmonic current to the stator harmonic winding which eventually created harmonic flux for brushless excitation.

A thyristor firing board and three antiparallel thyristor modules were used for the thyristor switching circuit as shown in Fig. 14 (a). For brushed operation, the machine was

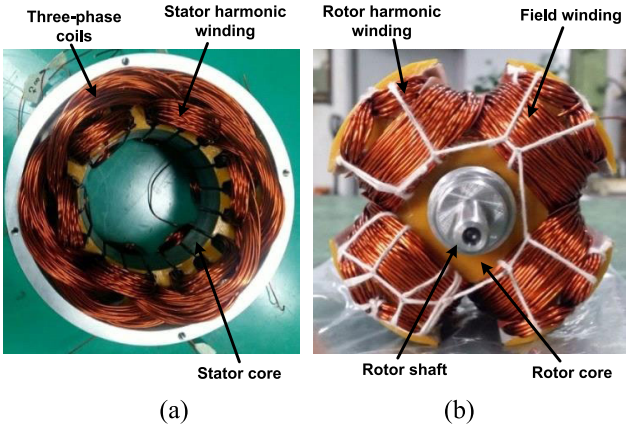

FIGURE 13. Prototype machine: (a) stator and (b) rotor.

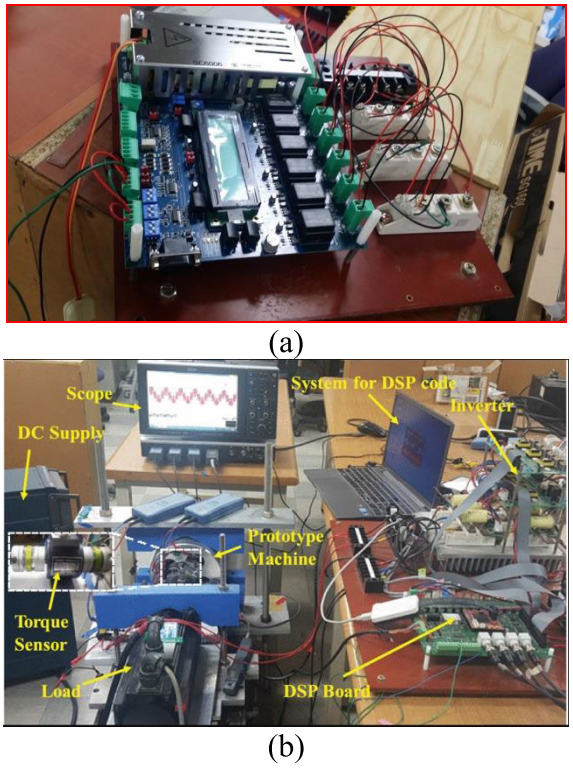

FIGURE 14. Experiment using the prototype machine: (a) thyristor firing board with thyristor modules and (b) setup for load-connected operation of the machine.

operated using the setup shown in Fig. 14 (b) and then the thyristor circuit was connected to the machine for brushless operation.

The experimental setup as shown in Fig. 14 (b) displays the prototype machine connected to a synchronous machine denoted as "Load". This synchronous machine was further connected to three-phase load resistances. Due to the absence of residual magnetism, the load machine was used to start the rotate the prototype machine to the rated speed and then the load machine was connected to resistive load. The torque in the load connection condition was measured by coupling the load with the prototype machine through a torque sensor.

To verify that the proposed brushless topology works through experiment on a prototype, a load torque should be obtained by providing the dc current to the stator harmonic winding from thyristor switching circuit. The experiment results in the steady state condition of the machine are shown in Fig. 15. The machine was supplied with currents from the inverter and the thyristor circuit was connected in parallel with the armature coils.

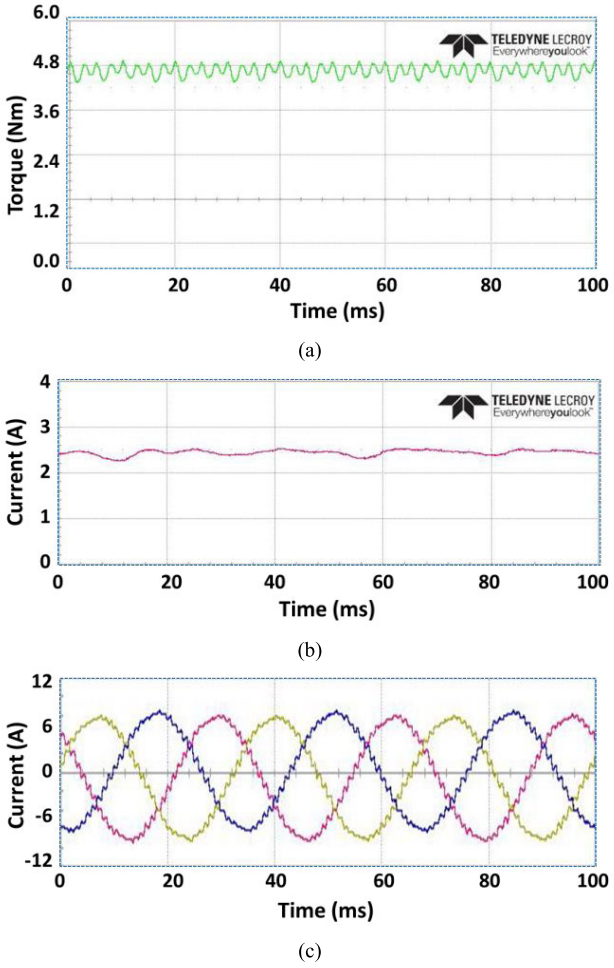

FIGURE 15. Experimental measurement (a) Torque of the machine (b) dc current fed to stator harmonic winding (c) Three phase currents from inverter.

In the experiment, the three-phase line currents were supplied to the machine at constant 60 Hz frequency. For controlled conditions, the inverter was used to supply a controlled fixed frequency. Three phase line currents are shown in Fig. 15 (c). The DC current fed to the stator harmonic winding and the torque are also shown in Fig. 15.

The torque of the machine was measured for brushless operation of the prototype. Fig. 15 (a) shows the measured torque in brushless operation in a steady state condition. It can be observed that the torque waveform shows ripples. These are mainly 6th and 12th harmonic order torque ripples. Other higher harmonic ripples were not clearly observed in

the experiment due to some neglected factors such as the rotor inertia which provides mechanical damping for torque ripple in the experiment. The torque output was measured to be 4.5 Nm in the brushless steady state condition with a torque ripple of 13%. It can be noted that the torque ripple in the experiment is lower than the torque ripple in the simulation. The smoother torque curve in the experimental result is mainly due to the coupled load machine which has its own inertia and the accumulated error in the experimental setup. The overall performance comparison is shown in Table 2. The measured torque of the machine in its steady state condition of brushless operation was is 4.5 Nm in the experiment whereas the torque was calculated as 4.6 Nm in simulation results. Therefore, a 2.2 % error was observed in the measured torque.

TABLE 2. Performance comparison parameters.

Parameter	(Unit)	Topology		
		Basic Topology Simulation	Proposed Topology Simulation	Proposed Topology Experiment
Phase Current	A	4.95	4.95	4.95
Phase Voltage	V	66	66	63
Field Current	A	4.1	4	3.85
Stator Harmonic Winding Current	A	-	2.4	2.4
Copper loss	W	67.6	102.5	100.8
Torque	Nm	5	4.6	4.5
Torque Ripple	%	70	15	13
Efficiency	%	0.89	0.85	0.83
Power Factor	-	0.9	0.9	-
Rotor Volume	L	0.5	0.5	0.5
Torque Density	Nm/L	10	9.2	9

A comparison is given in Table 2 showing that the input parameters are the same - that is 4.95 Arms phase current. The primary difference between the proposed topology and to the basic topology was that the induced field current and accordingly the torque was reduced.

V. CONCLUSION

This study proposed a brushless WRSM topology which employed a stator harmonic winding to control the harmonic current with thyristor switches without the use of an inverter. A stator harmonic winding was mounted on the stator in association with the armature winding for its configuration in a six-pole arrangement. Currents in the winding and switches in the proposed topology for brushless WRSMs were analyzed theoretically, and finite-element analyses were performed for verification of the brushless operation. The results obtained from the simulation and experiment were consistent and validated the operation of the proposed brushless WRSM. Therefore, it is concluded that the proposed topology works without an inverter and the unwanted harmonic content is low, which eventually results in low torque ripple. The results show that the topology has potential for implementation in a practical application. For further analysis, it can be implemented with specific load requirements and intensive tests can be performed to vary its capacity for application.

REFERENCES

[1] D. G. Dorrell, "Are wound-rotor synchronous motors suitable for use in high efficiency torque-dense automotive drives?" in *Proc. 38th Annu. Conf. IEEE Ind. Electron. Soc.*, Montreal, QC, Canada, Oct. 2012, pp. 4880–4885.

[2] G. J. Sirewal, T. A. Lipo, and B.-I. Kwon, "Torque ripple reduction in brushless wound rotor synchronous machine by two-phase excitation winding," *Int. J. Appl. Electromagn. Mech.*, vol. 59, no. 2, pp. 765–773, Mar. 2019.

[3] M. Ayub, A. Hussain, G. Jawad, and B.-I. Kwon, "Brushless operation of a wound-field synchronous machine using a novel winding scheme," *IEEE Trans. Magn.*, vol. 55, no. 6, Jun. 2019, Art. no. 8201104.

[4] G. J. Sirewal, M. Ayub, and B. Kwon, "A self-excitation topology for a brushless synchronous generator," in *Proc. 10th Int. Conf. Power Electron.*, Busan, South Korea, 2019, pp. 1227–1232.

[5] C. Chakraborty, S. Basak, and Y. T. Rao, "Synchronous generator with embedded brushless synchronous exciter," *IEEE Trans. Energy Convers.*, vol. 34, no. 3, pp. 1242–1254, Sep. 2019.

[6] M. Aoyama and T. Noguchi, "Rare-Earth free motor with field poles excited by space harmonics 2014; Current phase-torque characteristics of self-excitation synchronous motor," in *Proc. Int. Conf. Renew. Energy Res. Appl. (ICRERA)*, Madrid, India, Oct. 2013, pp. 149–154.

[7] K. Inoue, H. Yamashita, E. Nakamae, and T. Fujikawa, "A brushless self-exciting three-phase synchronous generator utilizing the 5th-space harmonic component of magneto motive force through armature currents," *IEEE Trans. Energy Convers.*, vol. 7, no. 3, pp. 517–524, Sep. 1992.

[8] F. Yao, Q. An, X. Gao, L. Sun, and T. A. Lipo, "Principle of operation and performance of a synchronous machine employing a new harmonic excitation scheme," *IEEE Trans. Ind. Appl.*, vol. 51, no. 5, pp. 3890–3898, Sep. 2015.

[9] F. Yao, D. Sun, L. Sun, and T. A. Lipo, "Dual third-harmonic-current excitation principle of a brushless synchronous machine based on double three-phase armature windings," in *Proc. 22nd Int. Conf. Electr. Mach. Syst. (ICEMS)*, Harbin, China, Aug. 2019, pp. 1–4.

[10] F. Yao, Q. An, L. Sun, and T. A. Lipo, "Performance investigation of a brushless synchronous machine with additional harmonic field windings," *IEEE Trans. Ind. Electron.*, vol. 63, no. 11, pp. 6756–6766, Nov. 2016.

[11] Q. Ali, T. A. Lipo, and B.-I. Kwon, "Design and analysis of a novel brushless wound rotor synchronous machine," *IEEE Trans. Magn.*, vol. 51, no. 11, Nov. 2015, Art. no. 8109804.

[12] M. Ayub, S. Atiq, G. J. Sirewal, and B.-I. Kwon, "Fault-tolerant operation of wound field synchronous machine using coil switching," *IEEE Access*, vol. 7, pp. 67130–67138, 2019.

[13] A. Hussain, S. Atiq, and B.-I. Kwon, "Consequent-pole hybrid brushless wound-rotor synchronous machine," *IEEE Trans. Magn.*, vol. 54, no. 11, Nov. 2018, Art. no. 8206205.

[14] A. Hussain and B.-I. Kwon, "A new brushless wound rotor synchronous machine using a special stator winding arrangement," *Elect. Eng.*, vol. 10, pp. 1–8, Nov. 2017, doi: 10.1007/s00202-017-0662-8.

[15] G. Jawad, Q. Ali, T. A. Lipo, and B.-I. Kwon, "Novel brushless wound rotor synchronous machine with zero-sequence third-harmonic field excitation," *IEEE Trans. Magn.*, vol. 52, no. 7, Jul. 2016, Art. no. 8106104.

[16] J. S. Dr Chitode, "Single and three-phase AC/DC converters," in *Power Electronics*. Pune, India: Technical, 2009.

[17] F. Yao, Q. An, L. Sun, M. S. Illindala, and T. A. Lipo, "Optimization design of stator harmonic windings in brushless synchronous machine excited with double-harmonic-windings," in *Proc. Int. Energy Sustainability Conf. (IESC)*, Oct. 2017, pp. 1–6.

[18] S. S. H. Bukhari, G. J. Sirewal, F. A. Chachar, and J.-S. Ro, "Dual-inverter-controlled brushless operation of wound rotor synchronous machines based on an open-winding pattern," in *Energies*, vol. 13, p. 2205, Oct. 2020.

[19] M. Ayub, G. J. Sirewal, S. S. H. Bukhari, and B.-I. Kwon, "Brushless wound rotor synchronous machine with third-harmonic field excitation," *Electr. Eng.*, vol. 102, no. 1, pp. 259–265, Mar. 2020.

[20] A. K. Mondal, S. Basak, and C. Chakraborty, "Design of a 4/6-pole synchronous machine with embedded brushless synchronous exciter (SEBSE)," in *Proc. IEEE 28th Int. Symp. Ind. Electron. (ISIE)*, Jun. 2019, pp. 2553–2558, doi: 10.1109/ISIE.2019.8781368.

GHULAM JAWAD SIREWAL was born in Tando Allahyar, Pakistan, in 1988. He received the B.E. degree in electrical engineering, in 2011, the Postgraduate Diploma degree in electrical power engineering from the Mehran University of Engineering and Technology, Jamshoro, Pakistan, in 2012, and the Ph.D. degree in electronic systems engineering from Hanyang University, South Korea, in 2020. He is currently a Postdoctoral Researcher with the Energy Conversion Systems Laboratory, Hanyang University. His research interests include electrical machine design and control.

MUHAMMAD AYUB was born in Quetta, Pakistan. He received the B.S. degree from the Balochistan University of Information Technology, Engineering and Management Sciences (BUITEMS), Quetta, in 2008. He is currently pursuing the Ph.D. degree with the Department of Electrical and Electronic Engineering, Hanyang University, Ansan, South Korea. He was a Lecturer with BUITEMS. His research interests include electric machine design and control.

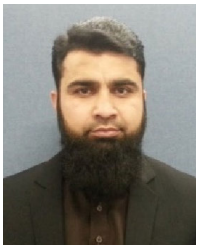

SHAHID ATIQ (Member, IEEE) was born in Pakistan. He received the bachelor's and master's degrees in electrical engineering from the University of Engineering and Technology Taxila, Pakistan, and the Ph.D. degree from the Energy Conversion Systems Laboratory, Hanyang University, South Korea. He is currently an Associate Professor with the Electrical Engineering Department, Khwaja Fareed University of Engineering and Information Technology, Rahim Yar Khan, Pakistan. His research interests include electrical machines design, drive, control, and power converters.

BYUNG-IL KWON (Senior Member, IEEE) was born in 1956. He received the B.S. and M.S. degrees in electrical engineering from Hanyang University, Ansan, South Korea, in 1981 and 1983, respectively, and the Ph.D. degree in electrical engineering, machine analysis from The University of Tokyo, Tokyo, Japan, in 1989. From 1989 to 2000, he was a Visiting Researcher with the Faculty of Science and Engineering Laboratory, Waseda University, Tokyo. In 1990, he was a Researcher with the Toshiba System Laboratory, Yokohama, Japan. In 1991, he was a Senior Researcher with the Institute of Machinery and Materials Magnetic Train Business, Daejeon, South Korea. From 2001 to 2008, he was a Visiting Professor with the University of Wisconsin–Madison, Madison, WI, USA. He is currently a Professor with Hanyang University. His research interests include design and control of electric machines.